23rd International Conference on Renewable Energies and Power Quality (ICREPQ'25)
Tenerife (Spain), 25th to 27th June 20245
Renewable Energy and Power Quality Journal (RE&PQJ)
ISSN 2172-038 X, Volume No.23, September 2025

Analysis of Grounding Systems Interference between Smart Tunnel and Electrical Distribution Grids

A. Fioravanti, A. Prudenzi, F. Ciancetta, E. Fiorucci and S. Mari

Department of Industrial and Information Engineering and Economics
University of L'Aquila
Piazzale Ernesto Pontieri, Monteluco di Roio, 67100 L'Aquila (Italy)

Abstract. The growing demand for services in urban areas, hidden from view, has spurred the development of innovative solutions such as the Smart Tunnel. This advanced infrastructure enables centralized and secure management of major city sub-services, including electricity, water and telecommunications networks, which are continuously subject to evolutions and upgrades. In addition, thanks to the Smart Tunnel configuration, maintenance interventions, modifications or the implementation of new connections are significantly simplified and more efficient. The issue of electrical safety, particularly with regard to grounding systems, plays a critical role in complex and widespread infrastructures such as these. In particular, the grounding systems of these tunnels have the potential to conflict with the grounding networks of the electrical distribution system. This study was undertaken to better understand the dynamics of interaction between the tunnel grounding system and nearby electrical distribution networks, with the ultimate goal of ensuring increasingly high safety standards.

Key words. Electrical distribution systems, electrical safety, FEM simulations, grounding systems, smart tunnel.

1. Introduction

The primary objective of this research is to analyze how the grounding system of a Smart Tunnel may interfere with nearby electrical distribution grids. Tunnel is a modern infrastructure that consolidates essential urban services, such as water, electricity, and telecommunications, within a single underground conduit, optimizing maintenance operations and network expansion without disturbing road surfaces. However, the presence of metal cable trays, conductors, shielding components, and structural elements, such as reinforcing bars in the tunnel walls and buried copper grounding cables, can lead to electrical interference, hazardous potential differences, and alterations in ground potential distribution [1,2].

The study focuses on evaluating these interactions and developing technical solutions to improve the safety and reliability of grounding systems.

The analysis has been conducted primarily through Finite Element Method (FEM) simulations, allowing for a detailed evaluation of the electromagnetic interactions within this complex infrastructure.

Section II examines grounding systems, with a particular focus on the grounding infrastructure of Smart Tunnels.

Section III describes the simulation process used to analyze ground potential distribution and electromagnetic interference issues.

These simulations provide a clear understanding of how each element affects the overall behavior of the grounding system.

Finally, Section IV presents and discusses the results obtained. The concluding part of the study summarizes the key findings from the simulations and outlines potential future developments.

2. Grounding Systems

Grounding systems are essential for the safety and functionality of electrical systems, ensuring protection for both people and equipment [3]. Their primary function is to provide a low-resistance path for fault currents, preventing electric shock hazards and potential damage.

Relevant regulations, such as CEI 64-8, CEI 0-16, CEI 0-21, and CEI EN 50522 [4], establish guidelines for the design and safety of low, medium, and high-voltage grounding systems. These systems connect non-energized metallic structures to the ground, ensuring that in the event of a fault, the current flows safely through the grounding system, preventing dangerous potential differences [5].

For instance, CEI 64-8 specifies the maximum permissible touch voltage and provides guidelines for the proper sizing of grounding systems, considering different fault scenarios.

The key objectives of grounding systems include:

- Protecting people from electric shocks,
- Preventing damage to electrical equipment,
- Reducing the risk of fires and malfunctions,
- Ensuring the reliable operation of electrical systems in complex environments.

In an urban environment, where the Distribution System Operator (DSO) supplies electricity through a TT system, multiple grounding systems can interact and interfere with each other. For example:

- The grounding system of the DSO's MV/LV substation, which is connected to the neutral conductor and the star point of the transformer's low-voltage side,
- The grounding system connected to MV cable shields,

- The grounding systems of individual homes or apartment buildings.

Additionally, urban areas also feature grounding systems for:

- Lightning protection systems,
- Telecommunications grounding,
- Protecting metallic structures from stray currents or galvanic corrosion,
- Preventing dangerous accumulations of electrical charges

These types of grounding systems can be either localized or distributed across the considered area. One of the main issues they can cause is step and touch voltages, which occur when the current does not properly disperse into the ground.

Various grounding configurations exist to address this challenge, including vertical electrodes, grounding rings, and mesh grids, which help ensure a uniform distribution of current in the soil.

In a complex urban environment, there is also a need to adapt the grounding system to accommodate the presence of underground structures, such as pipelines and cables.

A. Smart tunnel

The Smart Tunnel is a type of infrastructure designed to optimize the management of urban utility networks, allowing the passage of key services such as potable water, stormwater and wastewater drainage, medium and low-voltage power distribution, and telecommunications lines (Fig. 1).

Each system is housed in dedicated compartments within the tunnel, which is accessible on foot by technicians, making inspection and maintenance operations significantly easier. In the event of a failure, identifying and resolving the issue is straightforward, eliminating the need for disruptive roadwork.

Another key advantage is the ability to facilitate network connections through these ducts. This reduces installation costs as well as expenses associated with future network expansions.

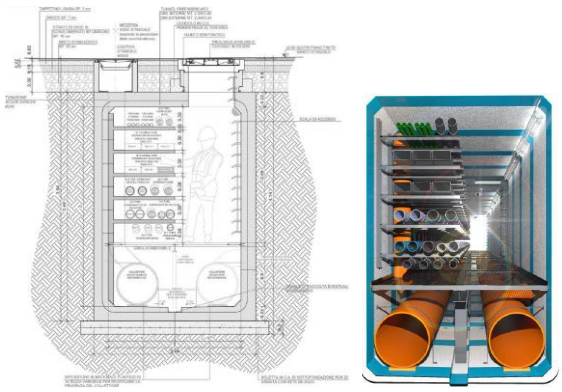

Fig. 1. Examples of a Smart Tunnel Cross-Section

An example of this infrastructure has been implemented in the historic center of L'Aquila (Italy), a city that was almost entirely rebuilt following the 2009 Central Italy earthquake. This infrastructure extends along the main streets for a total length of approximately 12 km, running beneath the road surface (Fig. 2).

Fig. 2. Smart Tunnel Distribution in the City Center of L'Aquila

The grounding system of the Smart Tunnel is generally implemented using one of two methods:

- A buried bare copper conductor placed beneath the tunnel.
- Ground rods driven into the soil below the tunnel floor.

The first approach is used when the grounding system is installed before the prefabricated tunnel modules are positioned. In this case, the copper conductor is laid approximately 50 cm deeper than the excavation level. Conversely, when the grounding system is implemented after the concrete structure has been completed, the second approach is adopted, using vertical ground rods.

These two configurations are classified as "intentional ground electrodes". Additionally, at grounding nodes, the reinforcing bars of the concrete structure are interconnected with the grounding system, forming "natural ground electrodes." This integration significantly contributes to reducing the overall ground resistance.

The grounding system is then connected to an insulated copper conductor running along a cable tray. To ensure equipotential bonding, all cable trays are interconnected, enhancing fault current dissipation towards the ground electrodes. However, these metallic structures pose a risk of dangerous touch voltages.

3. Method

It is important to emphasize that, in the case of complex grounding geometries, numerical analysis becomes essential, as the empirical formulas available in the literature are often derived under simplifying assumptions that may not hold in practical scenarios [6].

For this study, the Ansys software was used, which employs the FEM to solve partial differential equations related to the distribution of electric potential and current flow in both conductive and non-conductive materials[7,8].

Grounding systems are composed of various materials, including conductors, soil, concrete, and other subsurface components [9]. In the simulation, the grounding conductors were modeled as copper, with a relative permittivity of 1 and an electrical conductivity of 58 MS/m.

The electrical conductivity and relative permittivity of the soil are site-dependent properties that are typically determined through field measurements.

A. Ground resistance of a hemispherical electrode

To validate the FEM model, a hemispherical electrode was initially considered, ensuring it was sufficiently distant from the return electrode so that the current field could be approximated as radial. The ground resistance R_e of a hemispherical electrode can be computed as the sum of all elementary contributions [10]:

$$R_e = \int_{r_0}^{\infty} \frac{\rho dr}{2\pi r^2} = \frac{\rho}{2\pi r_0} \quad (1)$$

The model implemented in Ansys consists of a hemispherical copper electrode with a radius of 1 meter, embedded in a homogeneous soil with constant resistivity $\rho=100\ \Omega\cdot m$. The surrounding ground is modeled as a hemisphere with a radius of 300 meters, a value deliberately chosen to be significantly larger than the electrode itself. This ensures that the electric potential at the outer boundary is effectively zero, thereby minimizing edge effects.
A current of 100 A is injected into the grounding electrode in the simulations to evaluate the resulting potential distribution on the soil surface, extending from the electrode outward to a distance where the ground potential can be considered negligible.
To simulate the return electrode, a conductive shell was placed around the outer boundary of the hemispherical soil domain and assigned a fixed potential of $V=0$.

B. Ground resistance of the single vertical rod

The previous example is easy to analyze but impractical for grounding an electrical system. In real-world applications, grounding is typically achieved using ground rods, strips, rings, disks, ground mats, and other similar configurations.
A common type of grounding system consists of one or more vertical ground rods, typically ranging from 1.5 to 3 meters in length and 1.25 to 2.5 centimeters in diameter [11, 12].
By applying the method of images, the ground resistance of a tubular rod with radius r_0, length L, and its top buried at a depth h below the soil surface can be calculated using Equation (2), as proposed by [13]. Alternatively, it can be estimated using Equation (3) according to [14], or Equation (4) as proposed by [15]. Additional formulas found in [16] include Equations (5) and (6) [17].

$$R_e = \frac{\rho}{2\pi L} ln\left[\frac{L}{r_0}\sqrt{\frac{3L+4h}{L+4h}}\right] \quad (2)$$

$$R_e = \frac{\rho}{2\pi L}\left\{ln\left[\frac{2L}{r_0}\left(1+\sqrt{1+\left(\frac{r_0}{2L}\right)^2}\right)\right] + \frac{r_0}{2L} - \sqrt{1+\left(\frac{r_0}{2L}\right)^2}\right\} \cong \frac{\rho}{2\pi L}\left(ln\left[\frac{4L}{r_0}\right] - 1\right) \quad for\ L \gg r_0 \quad (3)$$

$$R_e = \frac{\rho}{4\pi L}\left(1+\frac{L}{L+H}\right) ln\left[\frac{2L}{r_0}\right] \quad (4)$$

$$R_e = 0.366\frac{\rho}{L}\left(log\left[\frac{3L}{2r_0}\right]\right) \quad (5)$$

$$R_e = \frac{\rho}{2\pi L}\left(ln\left[\frac{4L}{r_0}\right] - 1\right) \quad (6)$$

For the simulation, a copper cruciform ground rod was modeled with cross-sectional dimensions of 5 cm × 5 cm, a thickness of 5 mm, and a height of 1.5 meters. The lower end of the rod was tapered to a point. The rod was driven into the ground to a depth of 0.5 meters, and a current of 100 A was applied to its top surface to simulate current injection into the soil. The surrounding soil properties and boundary conditions were kept identical to those used in the previous case

C. Ground resistance of the buried copper conductor

A widely adopted and effective method consists in placing a horizontal grounding electrode inside the trench, typically made of bare aluminum or copper conductor with an appropriate cross-section.
When using a buried copper conductor, the resulting ground resistance depends on several factors, including the electrode length L, soil resistivity ρ, burial depth h, and conductor radius r_0 (Fig. 3).

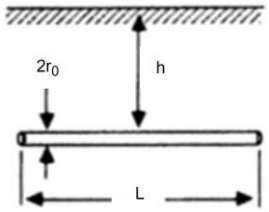

Fig. 3. Buried copper conductor

Ground resistance is a measure of the efficiency of a grounding electrode in dissipating fault current, and its accurate evaluation requires numerical techniques. A simplified formula for this grounding system is provided in Eq. (7) [18]. Alternatively, the image method can be applied using the formula presented in Eq. (8) [13].
In [16], the authors show Sunde's equation for calculating the resistance of a buried horizontal wire, as presented in Eq. (9). However, in his original book [14], Sunde provides a formula for a buried horizontal rod, as shown in Eq. (10).
It seems that there is an additional division by 2 in Eq. (9), likely due to a transcription mistake. As will be shown later, Eq. (9) produces a resistance value that is approximately half of those obtained using other methods.
Eq. (11) presents the formula for a buried horizontal wire of length $2l$ and burial depth $s/2$, as described in [19].
According to Conte [15], the ground resistance of a linear cylindrical electrode (buried wire) is expressed by Eq. (12).

$$R_e = \frac{\rho}{2\pi L}\left(ln\frac{L}{r_0} + ln\frac{L}{2h}\right) \quad for\ h \geq 6r_0 \quad (7)$$

$$R_e = \frac{\rho}{4\pi L}\left\{2ln\frac{L}{r_0} + ln\left[\frac{\frac{L}{2}+\sqrt{\left(\frac{L}{2}\right)^2+(2h+r_0)^2}}{-\frac{L}{2}+\sqrt{\left(\frac{L}{2}\right)^2+(2h+r_0)^2}}\right]\right\} \quad (8)$$

$$R_e = \frac{\rho}{2\pi L}\left[ln\left(\frac{2L}{\sqrt{2hr_0}}\right) - 1\right] \quad (9)$$

$$R_e = \frac{\rho}{\pi L}\left[ln\left(\frac{2L}{\sqrt{2hr_0}}\right) - 1\right] \quad (10)$$

$$R_e = \frac{\rho}{4\pi l}\left[ln\left(\frac{4l}{r_0}\right) + ln\left(\frac{4l}{s}\right) - 2 + \frac{s}{2l} - \frac{s^2}{16l^2} + \frac{s^4}{512l^4} \dots .\right] \quad (11)$$

$$R_e = \frac{\rho}{2\pi L}\left[ln\left(\frac{2L}{r_0}\right) + ln\left(\frac{L}{h}\right) - 2 + \frac{2h}{L}\right] \quad (12)$$

In the simulation, a buried conductor was modeled within the previously defined domain, positioned at a depth of 4.5 meters and with a total length of 10 meters. The conductor, made of bare copper, was assumed to have a perfectly cylindrical geometry with a cross-sectional area of 35 mm². A current of 100 A was applied as an outward flow from the surface of the conductor.

D. Smart Tunnel with a Vertical Ground Rod

In the subsequent test, a reinforced concrete tunnel structure was modeled with a length of 10 meters, a height of 3.5 meters, and a width of 2.1 meters. The wall thickness was set to 20 cm. The tunnel was embedded in the soil with its top surface located at a depth of 0.5 meters. A vertical ground rod, identical to the one analyzed in the previous test, was inserted at the center of the tunnel base.

An additional vertical ground rod, representing the earth electrode of a private electrical installation, was placed laterally to the tunnel at ground level. This electrode was intended to represent a portion of the earthing system of a private installation, which is assumed to be connected to all exposed conductive parts of the private building.

In the simulation, both the soil resistivity and the position of the private ground rod were varied in order to assess their impact on the global earthing resistance R_e, the step voltage, and the potential rise that could affect the connected equipment.

E. Smart Tunnel with a buried copper conductor

In the final test, the tunnel was equipped with an earthing system consisting of a buried horizontal conductor. The grounding electrode was implemented using a 10 meter long copper cylindrical conductor, buried at a depth of 4.5 meters (i.e., 0.5 meters below the base of the tunnel) with a cross-sectional area of 35 mm². A current of 100 A was then imposed, injected outward from the central section of the conductor.

4. Results

In this section, the results obtained through FEM simulations are presented and compared with the analytical solutions available in literature.

To compute the ground resistance, Ohm's law can be applied, relating the total ground voltage to the injected current [20]. Specifically, the ground resistance is defined as: $R_e=V_e/I$, where V_e is the potential difference between the electrode and a point at zero potential, and I is the current injected into the soil by the electrode. The zero-potential reference is theoretically located at an infinite distance from the electrode; however, in practical simulations, this condition is approximated by ensuring that the outer boundary of the soil domain is placed sufficiently far from the electrode, such that the potential at that boundary is negligibly small.

A. Ground resistance of a hemispherical electrode

The comparison between the FEM-based numerical results and the analytical expressions offers valuable insight into the accuracy of the models and emphasizes the influence of electrode geometry and positioning on the computed resistance.

Figure 4 presents the potential distribution obtained from the FEM simulation for the hemispherical electrode with a radius of 1 meter.

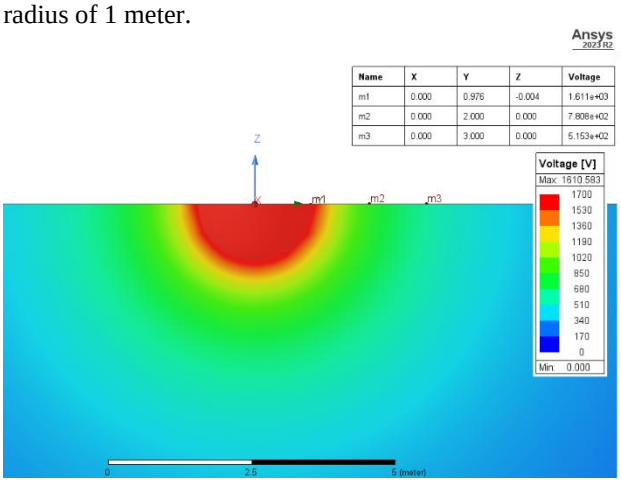

Fig. 4. Fem simulation of a hemispherical electrode

By evaluating the relationship between the voltage measured on the surface of the conductor and the injected current of 100 A, the ground resistance can be calculated and compared to the theoretical values derived from the analytical formula, as shown in Table 1.

The results clearly demonstrate that the FEM model closely matches the value obtained from the integral-based analytical solution, with only a negligible deviation attributable to numerical approximation errors.

Table I. - Comparison of Ground Resistance of a hemispherical electrode

Method	R_e	R_e / R_{eFEM}
Analytical formula	15.92 Ω	0.988
FEM Simulation	16.11Ω	1

B. Ground resistance of the single vertical rod

In the case of the vertical electrode, the results of the ground resistance calculations obtained using the FEM approach and the analytical formulas (Equations 2 to 6) are reported in Table 2.

It can be observed that the analytical expressions yield results that are in good agreement with the FEM simulations, with deviations ranging from approximately 2% to 8% higher.

Moreover, it is worth noting that Equation (2) explicitly accounts for the burial depth of the electrode, whereas this parameter does not appear in the other expressions. This is because many of the analytical formulas are derived under the assumption that the rod is flush with the ground surface, often by applying the method of images starting from the classical expression for capacitance, as reported in [21].

Table II. - Comparison of Ground Resistance of a single vertical rod

Method	R_e	R_e / R_{eFEM}
Eq. (2)	41.48 Ω	1.05
Eq. (3)	40.36 Ω (40.19)	1.02
Eq. (4)	42.74 Ω	1.08
Eq. (5)	40.33 Ω	1.02
Eq. (6)	40.19 Ω	1.02
FEM Simulation	39.48Ω	1

In most formulas, the electrode radius appears in the denominator of a logarithmic term, meaning its influence on the overall ground resistance is relatively limited. In the simulated case, the electrode has a cruciform cross-section with arms measuring 5 cm in width. For the values reported in Table 2, the width of the electrode was used as the equivalent radius.

The potential distribution on the plane intersecting the vertical electrode within the soil is shown in Figure 5.

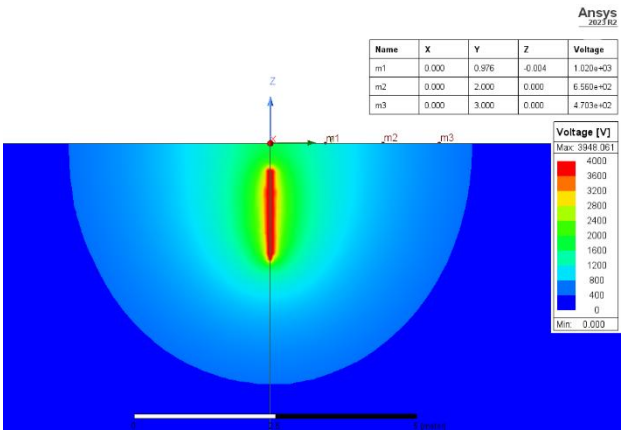

Fig. 5. Fem simulation of a single vertical rod

C. Ground resistance of the buried copper conductor

Table 3 presents the results obtained both analytically and through FEM simulations. In this case, some discrepancies are quite significant. Notably, there is a factor of two between the results of Equation (9) and Equation (10), which may be attributed to a transcription error. Despite its simplicity, Equation (10) provides the best agreement with the FEM simulation.

Table III. - Comparison of Ground Resistance of a buried horizontal wire

Method	R_e	R_e / R_{eFEM}
Eq. (7)	12.90 Ω	1.08
Eq. (8)	13.58 Ω	1.14
Eq. (9)	5.97 Ω	0.50
Eq. (10)	11.94 Ω	1.01
Eq. (11)	7.47 Ω	0.62
Eq. (12)	13.36 Ω	1.12
FEM Simulation	11.88 Ω	1

The increased percentage error observed in other formulas could be attributed to the assumptions made during their derivation, which may not align well with the specific conditions of our simulation. In fact, in our model, the horizontal conductor was buried at a depth of 4.5 meters, whereas typical installation depths are significantly shallower. This may explain the deviations, especially considering that in many formulas the burial depth h appears in the numerator and outside of logarithmic terms making the resulting ground resistance R_e highly sensitive to variations in h.

Figure 6 shows the potential distribution along two planes: the XZ radial plane, orthogonal to the conductor, and the YZ longitudinal plane, which intersects the conductor along its length. It is evident that the potential lines in the vicinity of the conductor form elliptical shapes, indicating that the distribution can no longer be accurately described using polar coordinates.

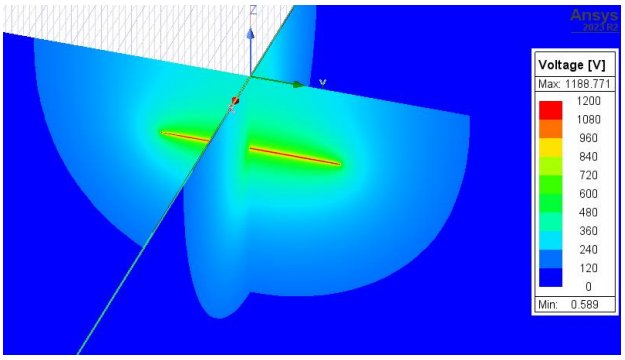

Fig. 6. Potential distributions for buried copper conductor

D. Simulation of a Tunnel with a Vertical Ground Rod

As shown in Table IV and figure 7, the earthing resistance is strongly influenced by the soil resistivity. Additionally, for ρ = 100 Ωm, the touch voltages measured at 2, 3, and 4 meters are considerably high and may pose a safety risk for people in the vicinity.

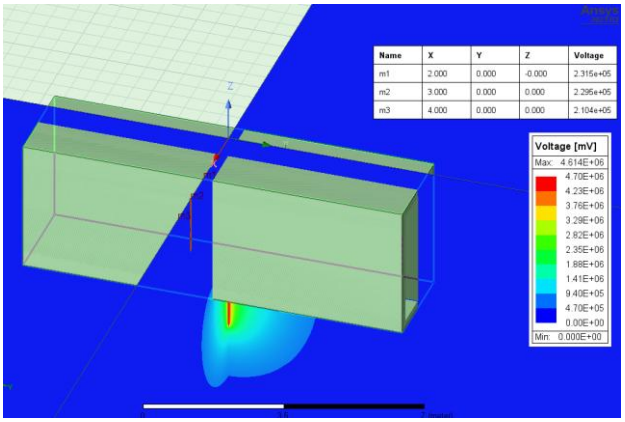

Fig. 7. Electric Potential Distribution near the Tunnel with One Vertical Rod and a Private Earth Electrode Spaced 3 m apart

For higher resistivity values, the calculated voltages exceed typical MV phase-to-ground values, which is physically unrealistic. This discrepancy is explained by the high earthing resistance, which results in reality in a fault current significantly lower than 100 A at the analyzed points in the case of an MV ground fault.

Furthermore, Table highlight that the presence of private ground electrodes increases the local ground potential, potentially bringing hazardous voltages to the exposed conductive parts of electrical equipment within nearby buildings. At the same time, the presence of a private vertical rod placed at 2 m, 3 m, or 4 m from the tunnel slightly affects the earthing resistance. This indicates that

the additional electrode does not significantly alter the global impedance of the tunnel earthing system.
Moreover, it can be observed that burying the vertical rod at a greater depth, respect to figure 5, contributes to a reduction in both step and touch voltages at the surface.

Table IV. - Influence of Soil Resistivity and Electrode Spacing on Earthing Parameters in the Tunnel with One Vertical Rod

Private Rod Distance		**Soil Resistivity [Ωm]**		
		100	500	1000
No private rod	**R_e [Ω]**	46.19	221.6	434.4
	V_{m1} [kV]	0.2312	1.088	2.128
	V_{m2} [kV]	0.2239	1.063	2.084
	V_{m3} [kV]	0.2100	1.003	1.972
Rod at 2 m	**R_e [Ω]**	46.27	222.6	434.4
	V_{m1} [kV]	0.2393	1.126	2.177
	V_{m2} [kV]	0.2248	1.070	2.084
	V_{m3} [kV]	0.2105	1.009	1.970
Rod at 3 m	**R_e [Ω]**	46.14	223.1	431.5
	V_{m1} [kV]	0.2315	1.097	2.114
	V_{m2} [kV]	0.2295	1.090	2.106
	V_{m3} [kV]	0.2104	1.011	1.961
Rod at 4 m	**R_e [Ω]**	46.16	224.8	436.4
	V_{m1} [kV]	0.2299	1.142	2.135
	V_{m2} [kV]	0.2295	1.078	2.106
	V_{m3} [kV]	0.2134	1.032	2.007

E. Simulation of a Tunnel with a buried copper conductor
The simulation results for the configuration with a buried copper conductor are reported in Table V and Figure 8. As can be observed, the earthing resistance (Re) is only marginally affected by the presence or absence of nearby private ground electrodes. Compared to Table III, however, Re is higher, indicating that the tunnel introduces a shielding effect that impairs the efficient dissipation of fault current into the surrounding soil.

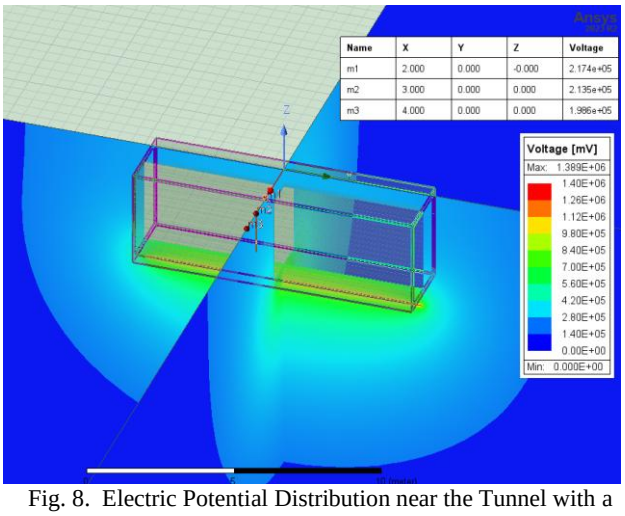

Fig. 8. Electric Potential Distribution near the Tunnel with a buried copper conductor and a Private Earth Electrode Spaced 2 m apart

The presence of the tunnel also contributes to an improvement in surface step and touch voltages measured at street level. Nevertheless, these voltages remain relatively high and must be carefully considered from a safety perspective.
As in previous cases, the presence of private ground rods induces a slight local overvoltage in their vicinity compared to the configuration without rods. This effect is more pronounced when the electrodes are placed closer to the tunnel, due to the localized increase in current density near their positions.

Table V. - Influence of Soil Resistivity and Electrode Spacing on Earthing Parameters in the Tunnel between a buried copper conductor and One Vertical Rod

Private Rod Distance		**Soil Resistivity [Ωm]**		
		100	500	1000
No private rod	**R_e [Ω]**	13.95	69.51	138.4
	V_{m1} [kV]	0.2202	1.102	2.208
	V_{m2} [kV]	0.2125	1.063	2.129
	V_{m3} [kV]	0.1999	0.9997	2.000
Rod at 2 m	**R_e [Ω]**	13.63	67.90	135.3
	V_{m1} [kV]	0.2251	1.105	2.256
	V_{m2} [kV]	0.2130	1.082	2.134
	V_{m3} [kV]	0.2000	1.002	2.003
Rod at 3 m	**R_e [Ω]**	13.53	67.45	134.4
	V_{m1} [kV]	0.2203	1.104	2.212
	V_{m2} [kV]	0.2126	1.082	2.164
	V_{m3} [kV]	0.2020	1.001	2.004
Rod at 4 m	**R_e [Ω]**	13.59	67.69	135.9
	V_{m1} [kV]	0.2203	1.103	2.212
	V_{m2} [kV]	0.2126	1.064	2.164
	V_{m3} [kV]	0.2020	1.011	2.004

5. Conclusion
The purpose of this work is to define a method for assessing soil resistance using Finite Element Method simulations in the context of smart tunnels. FEM offers the advantage of modeling more complex and realistic scenarios than those typically considered in standard calculations of earth resistance for different types of ground electrodes. As such, it is particularly well suited for analyzing the selected case study.
The model was first validated by comparing the simulated earth resistance of a hemispherical electrode with the well-known analytical expression. Subsequently, a similar comparison was carried out for a buried horizontal conductor, using analytical equations available in the literature. In most cases, the FEM results closely matched the analytical values, which generally provided conservative estimates from a safety perspective.
Particular attention was given to the implementation of a realistic portion of the smart tunnel, including the presence of construction rebar, and accounting for the electrical properties of the various materials involved in the model.
The results have shown how the earthing system interacts with neighboring grounding networks belonging to other users or distribution systems. This highlights the effectiveness of the proposed FEM-based method in evaluating phenomena that cannot be accurately captured through conventional analytical approaches.
A possible future development of this work involves modeling the soil as a multilayered medium with different resistivity values. The spatial distribution of resistivity can significantly affect the actual value of the ground resistance. One of the key advantages of FEM is precisely its ability to incorporate this type of complexity, ensuring a more accurate representation of the real behavior of the grounding system.

References

[1] G. Parise, L. Parise and L. Martirano, "The Interference of Grounding Systems: The Floating Behavior," in IEEE Transactions on Industry Applications, vol. 51, no. 6, pp. 5038-5043, Nov.-Dec. 2015, doi: 10.1109/TIA.2015.2443093.

[2] F. Freschi, M. Mitolo and M. Tartaglia, "Interferences phenomena between separate grounding systems," 2013 IEEE Industry Applications Society Annual Meeting, Lake Buena Vista, FL, USA, 2013, pp. 1-8, doi: 10.1109/IAS.2013.6682577.

[3] R. Guizán, I. Colominas, J. París, I. Couceiro, and F. Navarrina, "Numerical analysis and safety design of grounding systems in underground compact substations," Electric Power Systems Research, vol. 203, 2022, Art. no. 107627. [Online]. Available: https://doi.org/10.1016/j.epsr.2021.107627

[4] CEI EN 50522:2022-03. Earthing of power installations exceeding 1 kV a.c

[5] G. Parise and U. Grasselli, "Simplified conservative measurements of touch and step voltages," 1999 IEEE Industrial and Commercial Power Systems Technical Conference (Cat. No.99CH36371), Sparks, NV, USA, 1999, pp. 13-28, doi: 10.1109/ICPS.1999.787243.

[6] F. Freschi, M. Mitolo and M. Tartaglia, "An Effective Semianalytical Method for Simulating Grounding Grids," in IEEE Transactions on Industry Applications, vol. 49, no. 1, pp. 256-263, Jan.-Feb. 2013, doi: 10.1109/TIA.2012.2229688.

[7] C. Ma, S. Zhao, L. Sun, L. Wang, and G. Zhang, "THE Simulation Study of DC Grounding Electrode Based on CDEGS and ANSYS," *Journal of Physics: Conference Series*, vol. 1072, no. 1, p. 012006, 2018. doi: 10.1088/1742-6596/1072/1/012006.

[8] V. N. Katsanou and G. K. Papagiannis, "Substation grounding system resistance calculations using a FEM approach," *2009 IEEE Bucharest PowerTech*, Bucharest, Romania, 2009, pp. 1-6, doi: 10.1109/PTC.2009.5282044.

[9] A. Raizer, E. P. Elias, J. V. da Silva, M. V. F. da Luz, V. L. Coelho, V. M. A. Raupp, and M. Telló, "A comparative analysis of grounding in different structures: Operational vs. finite element method models," *Electric Power Systems Research*, vol. 230, p. 110243, 2024, doi: 10.1016/j.epsr.2024.110243.

[10] M. Brenna, F. Foiadelli, M. Longo and D. Zaninelli, "Particular grounding systems analysis using FEM models," 2018 18th International Conference on Harmonics and Quality of Power (ICHQP), Ljubljana, 2018, pp. 1-6, doi: 10.1109/ICHQP.2018.8378860.

[11] N. Chrisopolitis, T. Kollatou, D. Stimoniaris, and D. Tsiamitros, "Novel analytic EM field analysis and calculation formula for a ground resistance of a vertical ground rod in two-layer earth. Part I: Theoretical analysis," Electric Power Systems Research, vol. 230, 2024, Art. no. 110205, https://doi.org/10.1016/j.epsr.2024.110205

[12] L.-H. Chen, J.-F. Chen, T.-J. Liang, and W.-I. Wang, "Calculation of ground resistance and step voltage for buried ground rod with insulation lead," Electric Power Systems Research, vol. 78, no. 6, pp. 995–1007, 2008. https://doi.org/10.1016/j.epsr.2007.07.008

[13] V. Cataliotti, A. Campoccia, "Impianti di terra", Torino (TO), Italy, 2021.

[14] E. D. Sunde, Earth conduction effects in transmission systems. New York: Dover Publications Inc., 1968.

[15] G. Conte, Manuale di Impianti Elettrici, 3ª ed., Milano, Italy, Hoepli, 2020.

[16] Y. Al-Shawesh, S. C. Lim, and M. Nujaim, "Analysis of the design calculations for electrical earthing systems," nternational Review of Electrical Engineering (I.R.E.E.), vol. 16, no. 2, p. 104, Mar.-Apr. 2021. DOI: 10.15866/iree.v16i2.16839.

[17] J. Gómez, "Design and calculation of an earth electrode," in Proc. 3rd ST Workshop, Chamonix, France, Jan. 25–28, 2000, pp. 79–85, CERN-ST-2000-053.

[18] A. P. S. Meliopoulis, "Power System Grounding and Transients: An Introduction", 1st ed., New York, NY, USA: Routledge, 1988. DOI: 10.1201/9780203742686.

[19] Institute of Electrical and Electronics Engineers, IEEE Std-142 (Green Book): IEEE Recommended Practice for Grounding of Industrial and Commercial Power Systems, New York: IEEE, 2007.

[20] D. Liyanage and A. Rodrigo, "Estimation of Actual Earth Resistance in Complex Earthing Networks: A Case Study for Telecom Towers," *2022 36th International Conference on Lightning Protection (ICLP)*, Cape Town, South Africa, 2022, pp. 267-271, doi: 10.1109/ICLP56858.2022.9942516.

[21] Tagg,G. F., "Earth Resistance", England, George Newnes ltd, 1964.